

Tough, Transparent, 3D-Printable, and Self-Healing Poly(ethylene glycol)-Gel (PEGgel)

Zhenwu Wang, Haijun Cui, Modan Liu, Stephan L. Grage, Maxi Hoffmann, Elaheh Sedghamiz, Wolfgang Wenzel, and Pavel A. Levkin*

Polymer gels, such as hydrogels, have been widely used in biomedical applications, flexible electronics, and soft machines. Polymer network design and its contribution to the performance of gels has been extensively studied. In this study, the critical influence of the solvent nature on the mechanical properties and performance of soft polymer gels is demonstrated. A polymer gel platform based on poly(ethylene glycol) (PEG) as solvent is reported (PEGgel). Compared to the corresponding hydrogel or ethylene glycol gel, the PEGgel with physically cross-linked poly(hydroxyethyl methacrylate-*co*-acrylic acid) demonstrates high stretchability and toughness, rapid self-healing, and long-term stability. Depending on the molecular weight and fraction of PEG, the tensile strength of the PEGgels varies from 0.22 to 41.3 MPa, fracture strain from 12% to 4336%, modulus from 0.08 to 352 MPa, and toughness from 2.89 to 56.23 MJ m⁻³. Finally, rapid self-healing of the PEGgel is demonstrated and a self-healing pneumatic actuator is fabricated by 3D-printing. The enhanced mechanical properties of the PEGgel system may be extended to other polymer networks (both chemically and physically cross-linked). Such a simple 3D-printable, self-healing, and tough soft material holds promise for broad applications in wearable electronics, soft actuators and robotics.

These gels represent a class of soft materials with unique properties resembling soft biological tissues, such as tendons, ligaments, cartilage, muscles, and skin.^[6] Hydrogels, obtained by cross-linking hydrophilic polymer chains in aqueous solutions,^[7] possess the intrinsic low-modulus nature and tissue-like properties, which make them applicable to tissue engineering,^[8] optical devices,^[9] biomedicine^[10] and actuators.^[11]

In the pursuit of high performance, most research in the field of polymer gels has been focused on the chemical nature and polymer network architectures and their interactions,^[12] such as ideal polymer networks,^[13] interpenetrating polymer networks,^[14] nano/micro composite polymer networks,^[10,15] and hierarchically structured polymer networks.^[16] The small molecule solvent is the second component of gels and is often considered to be a non-functional liquid that impregnates and expands a functional polymer network.

Recently, ionic liquids have been used to replace water in hydrogels,^[17] resulting in soft materials with long-term stability.^[18] Multicomponent solvent systems, in which water is mixed with organic solvents (such as glycerol,^[19] ethylene glycol^[20] and sorbitol^[21]), were introduced into gel networks to maintain the performance of materials in harsh environments. However, because of the low molecular weight of solvents used and weak interactions with polymer networks, the reported

1. Introduction

Soft materials, benefiting from their low-modulus, deformable properties and diverse functionality, offer tremendous opportunities for applications in biomedicine,^[1] flexible electronics,^[2] soft robotics,^[3] and soft actuators.^[4] Polymer gels consist of physically or covalently cross-linked polymer chains and a liquid phase that is usually based on small molecule solvents.^[5]

Z. Wang, H. Cui, P. A. Levkin
Institute of Biological and Chemical Systems-Functional Molecular Systems (IBCS-FMS)
Karlsruhe Institute of Technology (KIT)
Hermann-von-Helmholtz-Platz 1, Eggenstein-Leopoldshafen 76344, Germany
E-mail: levkin@kit.edu

 The ORCID identification number(s) for the author(s) of this article can be found under <https://doi.org/10.1002/adma.202107791>.

© 2022 The Authors. Advanced Materials published by Wiley-VCH GmbH. This is an open access article under the terms of the Creative Commons Attribution-NonCommercial License, which permits use, distribution and reproduction in any medium, provided the original work is properly cited and is not used for commercial purposes.

DOI: 10.1002/adma.202107791

M. Liu, E. Sedghamiz, W. Wenzel
Karlsruhe Institute of Technology (KIT)
Institute of Nanotechnology
Hermann-von-Helmholtz-Platz 1, Eggenstein-Leopoldshafen 76344, Germany
S. L. Grage
Karlsruhe Institute of Technology
Institute for Biological Interfaces IBG-2
Hermann-von-Helmholtz-Platz 1, Eggenstein-Leopoldshafen 76344, Germany
M. Hoffmann
Karlsruhe Institute of Technology (KIT)
Institute for Chemical Technology and Polymer Chemistry (ITCP)
Engesserstraße 18, Karlsruhe 76131, Germany
P. A. Levkin
Karlsruhe Institute of Technology (KIT)
Institute of Organic Chemistry (IOC)
Kaiserstraße 12, Karlsruhe 76131, Germany

“organo-hydrogels” possessed limited mechanical properties and showed spontaneous solvent leakage.^[20] Furthermore, small molecules used as solvents in gels have limited number of possible interaction sites with the polymer network as well as with other solvent molecules. Here, we demonstrate that the use of liquid oligomers or polymers as solvents for gel systems offers the potential to introduce multivalent interactions between the main polymer network as well as between other solvent molecules. This approach can be used to significantly change the mechanical properties and stability of polymer gels. Importantly, such multivalency can be applied to enhance and finetune the physical properties of gels by changing the length of such oligomeric solvent molecules.

At room temperature, poly(ethylene glycol) (PEG) is a liquid ($M_w < 600 \text{ g mol}^{-1}$),^[22] which has been widely used in chemistry, biology, biotechnology and medicine^[23] and is currently approved for in vivo applications by the US Food and Drug

Administration.^[24] In blends with polymers possessing side hydroxy groups, PEG was shown to provide strong hydrogen bonding between main chain ether groups and hydroxy groups.^[25]

Here, we report a polymer gel system (PEGgel) based on a poly(hydroxyethyl methacrylate-*co*-acrylic acid) (P(HEMA-*co*-AAc)) network copolymerized in the presence of small- to average-molecular-weight PEG used as the liquid phase of the PEGgel (Figure 1a). Compared to the corresponding hydrogel generated using water or ethylene glycol as the liquid phase, the use of macromolecular non-volatile PEG results in a PEGgel with exceptional physical properties, such as high stretchability and toughness, rapid self-healing, and long-term stability under ambient conditions. Depending on the molecular weight and volume fraction of PEG, the tensile strength of PEGgels varied from 0.22 to 41.3 MPa, fracture strain from 12% to 4336%, modulus from 0.08 to 352 MPa, and toughness from 2.89 to

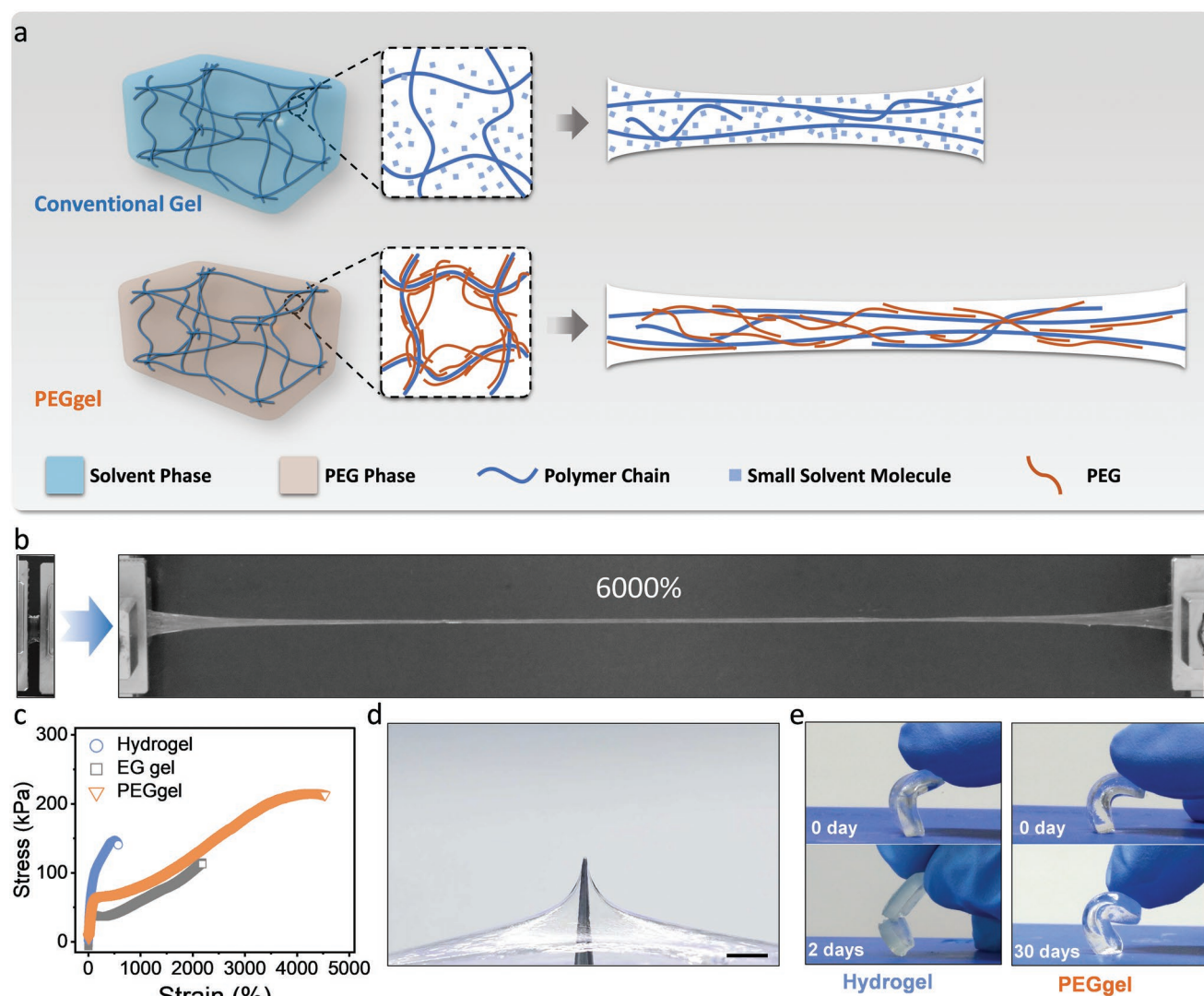


Figure 1. Concept of PEGgels. a) Schematic illustration of the hydrogel and PEGgel structure. b) Photographs of PEGgel stretched 6000%. c) Representative tensile stress–strain curves of hydrogel, PEGgel, and EG gel based on the same P(HEMA-*co*-AAc) polymer matrix and 50% solvent fraction. d) Photograph of a PEGgel membrane deformed by a sharp metal pin (pin diameter = 1 mm). Scale bar: 10 mm. e) Hydrogel and PEGgel blocks bent immediately after preparation and after storage for 2 days and 30 days, demonstrating the long-term stability of the PEGgel compared with that of the hydrogel.

56.23 MJ m⁻³. The influence of PEG on the mechanical properties was evaluated using the coarse-grain molecular dynamics (CGMD) model and solid-state NMR. Finally, we demonstrated rapid self-healing (≈ 1 min) and the possibility for 3D printing, by which the self-healing pneumatic actuator was fabricated. This study clearly demonstrates the important influence of the liquid phase of polymer gels on their mechanical and other properties, and highlights the potential for finetuning different physical properties of gels through the use of low-to-average molecular weight liquid polymers (e.g., PEG) possessing multiple hydrogen-bond interactions with the polymer network. Such a simple soft material holds promise for broad applications in wearable electronics, soft actuators and robotics.

2. Results and Discussion

2.1. Concept of PEGgels

PEGgel and the corresponding ethylene glycol (EG) gel and hydrogel were synthesized by free radical copolymerization of 2-hydroxyethyl methacrylate (25 vol%) and acrylic acid (25 vol%) dissolved in PEG ($M_w = 400$ g mol⁻¹), EG or water (50 vol%), respectively, in the presence of a radical initiator. The prepolymer solutions were poured into a poly(tetrafluorethylene) mold and cured by UV irradiation for 30 min (6 mW cm⁻², 366 nm, room temperature). After polymerization, the gel blocks were detached from the mold and used for further investigations. The polymerization was confirmed by the FTIR analysis (Figure S1, Supporting Information), where the 1633 cm⁻¹ band corresponding to the stretching of the C=C bonds of the monomers disappeared after polymerization. The obtained PEGgel was immersed in PEG400 (containing 1 mg mL⁻¹ Sudan I) for one week. After one week soaking, the diameter of PEGgel swell from 20 into 40 mm (Figure S2, Supporting Information), which confirms that the PEG is serving as fluid in polymer network. The obtained PEGgel could be stretched to 6000% of its original length at a rate of 50 mm min⁻¹ without rupture (Figure 1b), while the corresponding hydrogel could be stretched to only 400% without damage. To confirm the enhancement of the mechanical properties of PEGgels, we compared the performance of hydrogel, PEGgel and EG gel in tensile tests (Figure 1c). All three samples were based on P(HEMA-co-AAc) with the same monomers: solvent volume ratio (1:1) and identical polymerization conditions (Table S1, Supporting Information). After changing the solvent to PEG, the PEGgel showed a fracture strain of $4335 \pm 340\%$ and a tensile strength of 218 ± 16 kPa, while the corresponding hydrogel ruptured at $617 \pm 175\%$ and 150 ± 9 kPa and EG gel ruptured at $2382 \pm 192\%$ and 106 ± 8 kPa. The elastic modulus of PEGgel (78 ± 13 kPa) is similar with EG gel (76 ± 9 kPa), but lower than the hydrogel (125 ± 32 kPa). Notably, the toughness of PEGgel was 5.66 ± 0.58 MJ m⁻³, representing to a 9.1-fold increase compared with the corresponding hydrogel (0.62 ± 0.06 MJ m⁻³) and a 4.2-fold increase compared with the corresponding EG gel (1.35 ± 0.09 MJ m⁻³). In addition, rheological master curves of frequency dependence of the storage modulus (G') and loss modulus (G'') at a reference temperature of 25 °C for PEGgel, EG gel and hydrogel were presented in Figure S3

(Supporting Information). The G' of all the gels presented higher than G'' in the low-frequency region ($\omega \rightarrow 0$) without obvious crossover, which shows the dominant elastic behavior of P(HEMA-co-AAc) chains due to the physical crosslinks. Interestingly, PEGgel and EG gel presented an obvious narrowing of G' and G'' in the low frequency region, while $G' > G''$ still indicating dominant elastic behavior and no transition to the flow regime. Meanwhile, the hydrogel remained open toward the low frequency region, showing a wide rubber plateau due to the strong physical cross-linking. These different trends indicated that the polymer chains are most mobile in EG gel, followed by PEGgel and most fixed in hydrogel, which is also consistent with the tensile properties of the gels in three solvent systems.

The extreme toughness of the PEGgel was also reflected in the excellent mechanical durability of this soft and elastic material demonstrated in the piercing test, in which tip of a stainless-steel pin (diameter, 1 mm) was used to pierce a gel membrane (14×30 mm in size and 2.5 mm thick) at a speed of 100 mm min⁻¹. The pin stretched the PEGgel membrane 4.5 cm above the membrane plane without piercing it, while the P(HEMA-co-AAc) hydrogel membrane was pierced when stretched only 1.5 cm by the pin (Movie S1: Supporting Information and Figure 1d), demonstrating the high toughness of the PEGgel in comparison to the hydrogel. The absence of phase separation between the liquid PEG and P(HEMA-co-AAc) matrix was confirmed by the lack of visible light scattering and >95% transmittance of the PEGgel in the visible range (400–760 nm) (Figure S4, Supporting Information).

Stability in open environment is also crucial for soft materials. To determine the stability of PEGgels, the hydrogel and PEGgels were stored in open air (25 °C, 50% relative humidity) for 30 days. Due to the negligible evaporation from PEG, the PEGgel retained its flexibility for 30 days. The corresponding hydrogel became brittle after just 2 days and ruptured immediately upon bending, demonstrating the superior long-term stability of the PEGgel compared with the corresponding hydrogel (Figure 1e and Movie S2: Supporting Information). The weight changes of PEGgel and hydrogel were recorded during storage of the gels in open air (25 °C, $50 \pm 5\%$ relative humidity) over 30 days (Figure S5, Supporting Information). The weight of PEGgel remained unchanged ($\pm 1\%$), whereas the hydrogel lost 48% of its mass after one day, leading to the deterioration of its mechanical properties. After one month in storage under these conditions, the tensile stress–strain curve of PEGgel remained almost unchanged (Figure S6a, Supporting Information), the strength decreased only marginally from 218 to 200 kPa and the fracture strain was 3200%. In contrast, the fracture strain of the corresponding hydrogel decreased from 460% to 11% after only one day (Figure S6b, Supporting Information). The stability of PEGgels under different relative humidity was also investigated. EG gel and PEGgel were stored at 25 °C under saturated water vapor environment for 12 h (Figure S7, Supporting Information). Due to the higher density of hydroxyl groups, EG gel absorbed more water ($378 \pm 1.4\%$) than PEGgel ($9.6 \pm 1.5\%$) until reaching a balance. In the case of EG gel, the water absorption resulted in the loss of the sample shape, while the shape of PEGgel did not change significantly. The weight change of PEGgel after storage at 25 °C for 12 h with different humidity was recorded in Figure S8a (Supporting Information),

which increased less than 5% at relative humidity up to 50%. The mechanical property of PEGgel also did not change even after incubating samples at 50% relative humidity for 12 h (Figure S8b, Supporting Information). The toughness of PEGgel after storage in saturated water vapor environment was still as high as $1.95 \pm 0.07 \text{ MJ m}^{-3}$, which was still higher than those of the as-prepared hydrogels and EG-gels. The FTIR analysis confirms accumulation of water in PEGgel (Figure S9c, Supporting Information), which was most pronounced for 75% and 100% humidity.

2.2. Molecular Mechanism of PEGgels

To investigate the polymer network–solvent interactions within the gels and to clarify the molecular mechanisms underlying the experimentally observed mechanical properties of the gels, we have developed a coarse-grained (CG) molecular dynamics (MD) model. In the coarse-graining process illustrated in Figure S9 (Supporting Information), the individual polymer chains were represented by beads for the polymer backbone and side-groups, whereas water and EG was represented by single spherical beads. PEG was modeled as a short linear chain with the same resolution as EG. All the CG beads were capable of forming either O–H...O or C–H...O hydrogen bonds, with the latter found to be essential to model the PEG conformation.^[26] Full details of the CGMD simulation process, as well as the corresponding reduced units as λ_{CG} and ϵ_{CG} , are presented in the Methods section.

The relaxed conformations of a single polymer chain of poly(2-hydroxyethyl methacrylate-*co*-acrylic acid), or P(HEMA-*co*-AAc) exhibited strikingly different behaviors when solvated in water, EG, and PEG (Figure 2a). The single polymer chain was the most compact in water, due to the hydrophobicity of the polymer backbone, while OH side-groups were exposed to form hydrogen bonds with water. In EG, all the molecular units were of similar miscibility and the single polymer chain remained as a polymer coil. When solvated in PEG, the short, linear PEG molecules wrapped around the P(HEMA-*co*-AAc) and served as mitigators in the polymer–PEG–polymer cross-linking. Figure 2b shows a snapshot highlighting an individual PEG molecule (bright red) forming H-bonds at both ends to connect different sites of a single P(HEMA-*co*-AAc) chain. In contrast to EG, PEG molecules in the polymer–solvent–polymer cross-links effectively introduced long-range correlations, thereby enhancing compaction of the polymer coil. The radii of gyration of the single polymer chains measured $4.90 \lambda_{CG}$, $12.62 \lambda_{CG}$ and $10.36 \lambda_{CG}$ in water, EG, and PEG, respectively. The polymer–polymer interaction potential in water was much stronger (2 \times) than that of EG and PEG, indicating a polymer–water separation. Due to the high number of hydrogen donor and acceptor pairs in water, both the polymer–solvent and the solvent–solvent interaction energies in water were an order of magnitude larger than those in EG and PEG. In contrast, due to the similar miscibility of the polymer backbone and side groups in EG and PEG, the polymer uniformly mixed with the solvent molecules, leading to an open conformation of the solvated single polymer chain. The polymer–polymer interaction in PEG was just 8.5% larger than that in EG. Compared with the small,

spherical water and EG molecules, the large PEG molecules have reduced freedom of diffusion, which restrained the conformation of the P(HEMA-*co*-AAc) chains even in the dilute limit.

In CGMD simulations^[27] of the elongation process up to 5000%, we found that the strain–stress response of the polymer network was qualitatively consistent with the experimental data (Figure 1c and Figure S10a: Supporting Information). In the gel system, the CGMD simulations revealed different contributions to the overall mechanical response of the hydrogel, EG gel, and PEGgel upon stretching. A comprehensive analysis of the componential energy contribution from steric repulsion, hydrogen bonding and covalent bonds is presented in Figure 2c and Table S10 (Supporting Information). As for the solvation of single polymer chains, hydrogen bonding was the predominant contributor in the gel systems. Compared with the EG gel and PEGgel, the more inhomogeneous distribution of the water molecules in the hydrogel indicated a stronger polymer–solvent separation (Figure S10b, Supporting Information). This led to a stiff mechanical response when the hydrogel got stretched.

In stark contrast, the polymer network in the EG gel remained homogeneously mixed at the molecular scale during the stretching process (Figure S10c, Supporting Information). The EG solvent served as a mitigating medium linking the polymer chains, albeit in the form of short-range polymer–EG–polymer cross-links. Compared to water, the hydrogen bonding was less prevalent in the EG gel, leading to a soft response to the external stretching. The behavior of the PEGgel lay between the hydrogel and EG gel. The unique C–H...O hydrogen bond in the PEGgel was the predominant contributor to the hydrogen-bond energy. The PEGgel had fewer OH groups compared to the hydrogel and EG gel as the OH groups from the solvent were located only on the termini of PEG. While the C–H...O bond was weaker than the O–H...O bond, the large number of ether groups on the PEG molecules facilitated frequent formation of C–H...O hydrogen bonds. The contribution from the H-bonds between the OH group on the polymer and the ether group of PEG ($0.107 \epsilon_{CG}$) is $9 \times$ smaller than that of the C–H...O bond energy ($0.97 \epsilon_{CG}$). Among the three solvents, the total energy from the hydrogen bonding was the weakest in PEG. However, between the EG gel and PEGgel, the greater C–H...O H-bond energies in the PEG corresponded to a much larger number of H-bonds, which compensated for most of the energy difference. Overall, the presence of such frequent but weak cross-linking sites facilitated a pronounced polymer–polymer cross-linking.

Moreover, the larger size of the PEG molecule, enhanced by the intramolecular hydrogen bonding, causes the solvent molecules to occupy distinct spaces among the polymer chains, thereby leading to local compression of the polymer network into a less homogeneously distributed pattern (Figure S10d, Supporting Information). To quantify the entanglement, we calculated the ensemble contour lengths for the polymer networks of the hydrogel, the EG gel and the PEGgel at 550% stretching using the Z1 method.^[28] The contour length is a measure for the number of polymer units where the polymer has avoided the presence of another chain. A snapshot of the polymer network, with the highlighted entanglement sites between two polymer chains, is shown in Figure S10e (Supporting Information).

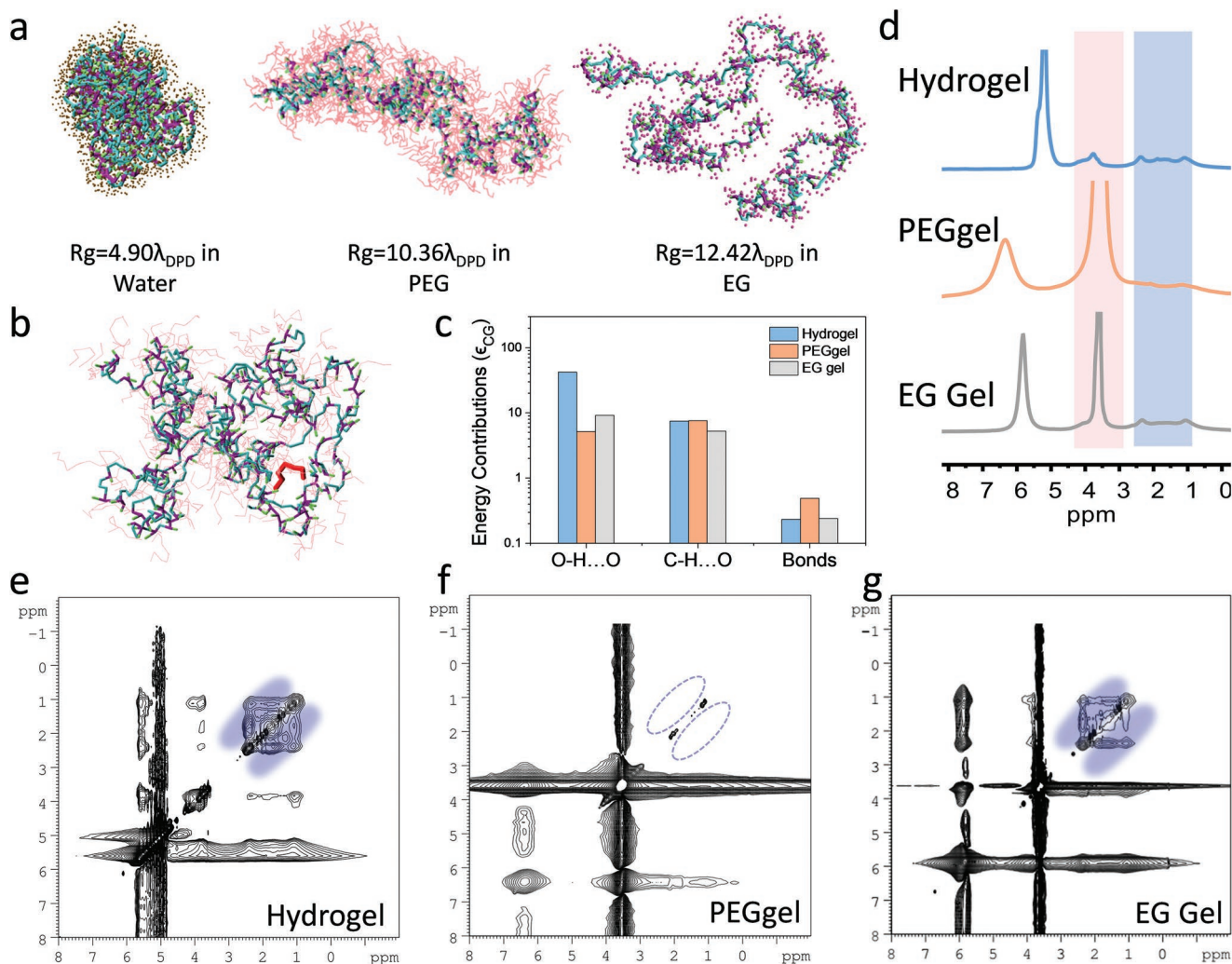


Figure 2. The CGMD simulation and the solid-state NMR investigation of the gel systems. a) CGMD simulated single-chain conformations of P(HEMA-co-AAc) in water, PEG, and EG (from left to right). Size of the single chain, characterized by the calculated radius of gyration for the single-chain polymer. Atom groups in HEMA-co-AAc are color coded in accordance with the CG scheme in Figure S9 (Supporting Information). The solvent in the immediate vicinity of the polymer is shown as tan-colored dots for water, violet-colored dots for PEG, and pink short chains for PEG. b) A snapshot of the polymer-PEG-polymer cross-linking via H-bonding for the single P(HEMA-co-AAc) chain in PEG. The PEG highlighted in red forms an intrapolymer cross-linking unit. c) Componential contributions to the interaction potentials of the O-H...O hydrogen bonding, C-H...O hydrogen bonding and covalent bonds in three gels stretched to 550%. d) Solid state MAS ^1H -NMR spectra of hydrogel (blue), PEGgel (orange), and EG gel (gray). e-g) Anticipated inter- and intrachain interactions are supported by 2D exchange ^1H -NMR experiments acquired under MAS using a mixing time of 100 ms of the hydrogel (e), PEGgel (f), and EG gel (g). The cross peaks arising from magnetization exchange between methyl groups ($-\text{CH}_3$) and copolymer backbone ($-\text{CH}_2-\text{CH}_2-$) in P(HEMA-co-AAc) are marked in blue, which connect the resonances at 1.1 and 2.4 ppm, respectively.

As summarized in Table S11 (Supporting Information), PEG has the shortest contour length, indicating a maximal polymer-polymer entanglement among the three gel systems. Larger entanglement is associated with improved mechanical properties,^[29] as long as there are no knots,^[30] which makes the polymer brittle.

To summarize, in the hydrogel, strong O-H...O hydrogen bonds and lack of miscibility with the solvent result in a stiff system. In the EG gel, the enhanced miscibility with the solvent means that EG can substitute easily for polymer-polymer interactions, resulting in a very soft system. For the PEGgel, the weak but abundant C-H...O hydrogen bonds generate a large number of variable interaction points that can accommo-

date the strain of the system. In contrast to the other two systems, the larger size of PEG generates more flexible long-range polymer-PEG-polymer cross-links. While these effects pertain to the scale of individual, the somewhat larger polymer entanglement in the PEGgel may also contribute somewhat to the improved mechanical properties^[29b] at longer length-scales.

To further elucidate the structural differences between the three gel systems, an in situ 2D solid state ^1H -NMR characterization of these three gels was performed (Figure 2d). Indeed, in the 2D exchange spectrum of the hydrogel (Figure 2e), cross peaks connecting signals at 1.1 and 2.4 ppm, which indicate magnetization exchange between the methyl groups ($-\text{CH}_3$) and the backbone ($-\text{CH}_2-\text{CH}_2-$) of P(HEMA-co-AAc), respectively,

can be clearly seen. In contrast, the cross peaks between 1.1 and 2.4 ppm were not observed in the case of the PEGgel (Figure 2f). We note at this point that the strong signals at 3.8 and 6.5 ppm arise from PEG, and would obscure potential cross peaks originating from the HEMA polymer. Nonetheless, the presence of spin diffusion within the HEMA polymer in the case of the hydrogel, and the absence of it in the PEGgel supports the proposed model of solvent–polymer interaction. The compact polymer clusters in the case of the hydrogel lead to restricted motion and close proximities of the hydrogens in the sample, resulting in strong ^1H – ^1H dipolar couplings and spin diffusion. In the PEGgel, on the other hand, the more elongated chains exhibit more motion and the hydrogens are further separated, leading to reduced spin diffusion. In the case of the EGgel, however, cross peaks between the methyl groups and the backbone within the HEMA polymers were again observed (Figure 2g). Again, the signals at 6.0 and 3.8 ppm are solvent peaks, restricting the analysis to the region of below ≈ 3 ppm. We further quantified the spin diffusion observed in the 2D exchange NMR experiments by analyzing the intensity of the cross peaks connecting the signals at 1.1 and 2.4 ppm as a function of the mixing time (Figure S11, Supporting Information). The mixing time is a delay in the experiment, during which exchange processes such as spin diffusion are occurring. The intensity of the cross peaks (sum of both) was related to the intensity of the diagonal peaks (sum of the signals at 1.1 and 2.4 ppm), and shows an increase with mixing time in the case of the hydrogel and EG gel, and nearly no cross peak intensity was detected in the case of the PEGgel. Thus, as opposed to water and EG in the hydrogel and EG gel, PEG seems to participate in the gel network formation with larger molecule size, which further results in the enhanced mechanical properties.

2.3. Tunable Mechanical Properties of PEGgels

To further investigate the effect of solvent on the mechanical properties of the gel systems, we varied the volume fraction of PEG and its molecular weight, thereby achieving tunability of the mechanical property of the P(HEMA-*co*-AAc) PEGgel (HAP). Prepolymer solutions of all samples (Tables S2 and S3, Supporting Information) were added into a mold and exposed to UV for 30 min (6 mW cm^{-2} , 366 nm, room temperature). All mechanical tests were performed in air, at room temperature, using a universal tester with a 100 N load cell and 100 mm min^{-1} load speed. We first evaluated the effect of PEG volume fraction on the mechanical properties of PEGgel (Figure 3a) using PEG 400 (400 g mol^{-1}) as a solvent. The tensile strength of the PEGgel obtained increased from 0.21 MPa (50 vol%) to 41.29 MPa (20 vol%) as the PEG 400 volume fraction decreased, while the fracture strain decreased from 4335% (50 vol%) to 12% (20 vol%). In addition, the elastic modulus of the gels showed a similar pattern of changes, increasing from 0.078 MPa (50 vol%) to 352 MPa (20 vol%) as the volume fraction of PEG 400 decreased. In addition, the toughness of PEGgel could be tuned solely by changing the volume fraction of PEG from 50% to 20%, from 5.66 MJ m^{-3} (50 vol%) to 2.89 MJ m^{-3} (20 vol%). The differential scanning calorimetry (DSC) analysis demonstrated same trend on T_g change, which depends on

the mobility of the polymer chains (Figure S12a, Supporting Information). With PEG volume fraction decreasing, the T_g of PEGgel increased from $-38.8\text{ }^\circ\text{C}$ (HAP-5) to $-27.0\text{ }^\circ\text{C}$ (HAP-4.5), $-25.2\text{ }^\circ\text{C}$ (HAP-4), $-15.2\text{ }^\circ\text{C}$ (HAP-3.5), $-8.2\text{ }^\circ\text{C}$ (HAP-3), $0.5\text{ }^\circ\text{C}$ (HAP-2.5), and $22.3\text{ }^\circ\text{C}$ (HAP-2). Here, lower volume fraction of PEG, serving as solvent, renders the polymer network less flexible, showing faster crack extension,^[31] resulting in the higher elastic moduli and lower fracture strain of the gel.^[13a]

Next, we evaluated the effect of the molecular weight of PEG used as a solvent on the mechanical properties of the PEGgel, with a constant PEG volume fraction of 60% (Figure 3b). The tensile strength of the PEGgel obtained with different PEGs increased from 0.60 MPa (PEG 200 g mol^{-1}) to 0.61 MPa (PEG 400 g mol^{-1}), 1.61 MPa (PEG 600 g mol^{-1}), and 2.20 MPa (PEG 1000 g mol^{-1}) as the molecular weight of PEG increased. However, as the molecular weight of PEG increased, the fracture strain of the PEGgel decreased from 2570% (PEG 200) to 1668% (PEG 400), 1244% (PEG 600), and 1280% (PEG 1000). The larger molecular weight of PEG provides more interactions among polymer chains of the network in the PEGgel, efficiently enhancing its tensile strength. In addition, the flexibility of the P(HEMA-*co*-AAc) polymer chain is reduced as the molecular weight of PEG increases, resulting in a further reduction in the fracture strain. Similarly, the elastic modulus and toughness of PEGgel can be tuned easily by changing the molecular weight of PEG. The difference on T_g of these PEGgels also confirmed this trend (Figure S12b, Supporting Information). With the larger PEG molecular weight, the T_g of PEGgel increased from $-48.2\text{ }^\circ\text{C}$ (HAP200) to $-25.2\text{ }^\circ\text{C}$ (HAP400), $-23.6\text{ }^\circ\text{C}$ (HAP600) and $-18.6\text{ }^\circ\text{C}$ (HAP1000). By increasing the molecular weight of PEG from 200 to 1000 g mol^{-1} , the elastic modulus and toughness of the corresponding PEGgels increased from 0.10 MPa and 7.36 MJ m^{-3} to 0.52 MPa and 9.99 MJ m^{-3} , respectively (Figure 3c,f). Moreover, cyclic tensile loading-unloading with gradual increase in strain was measured using HAP-4 (Figure S13, Supporting Information). The obvious hysteresis demonstrates the energy dissipation in PEGgel during loading-unloading cycles. The second, third and fourth loading curves almost overlapped with the previous ones, indicating a rapid recovery of the network despite the energy dissipation during loading. Such rapid recovery is likely attributed to the reversible and dynamic hydrogen bonding between the P(HEMA-*co*-AAc) chains and PEG, which temporarily ruptured to dissipate energy upon loading and rapidly reformed during unloading.

Thus, the mechanical properties of PEGgels were tuned by changing the volume fraction and molecular weight of PEG, with an available range of tensile strength, fracture strain, elastic modulus, and toughness of 0.22–41.3 MPa, 12–4336%, 0.08–352 MPa, and 2.89 – 56.23 MJ m^{-3} , respectively (Figure 3c–f). Notably, the elastic modulus of PEGgels can be tuned within a broad range, from near 0.08 to 352 MPa, which covers the Young's modulus of most tissues in the human body (Figure 3g),^[32] especially different skin types.^[33] Overall, the PEGgel showed high ultimate stress and strain that well covered the values seen in many reported tough hydrogels and elastomers (Figure S14 and Table S12, Supporting Information). With such a broad range of elastic moduli, PEGgel represents a highly promising material platform for the development of

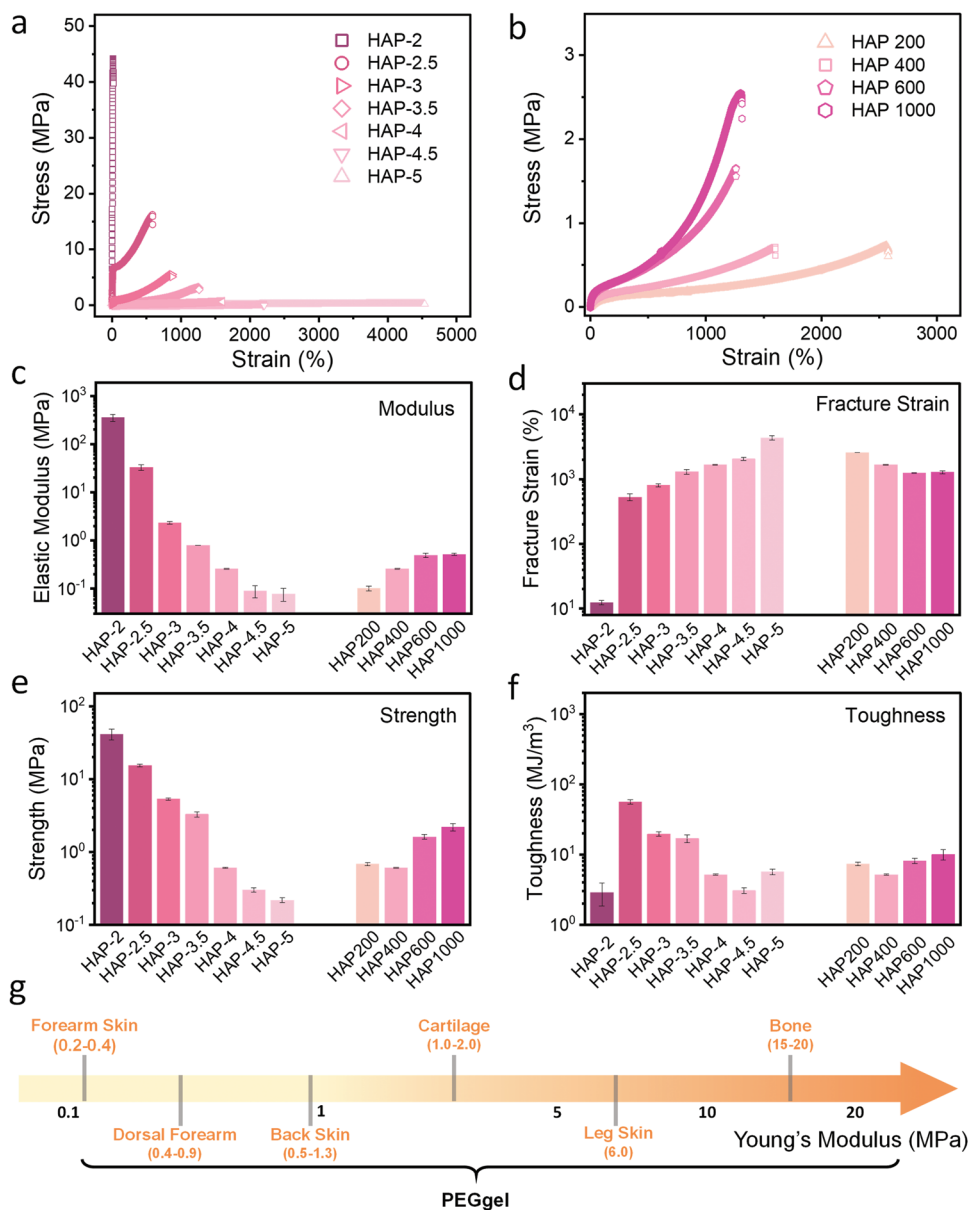


Figure 3. The tunable mechanical properties of PEGgel. a) Representative stress–strain curves of PEGgels containing PEG 400 with volume fractions ranging from 20 vol% (HAP-2) to 50 vol% (HAP-5). b) Representative stress–strain curves of PEGgels composed of PEG 200 (HAP 200), 400 (HAP 400), 600 (HAP 400) and 1000 (HAP 1000), with constant PEG fraction of 40 vol%. c–f) Modulus (c), fracture strain (d), strength (e), and toughness (f) of PEGgels mechanically tuned based on variation of PEG types and volume fractions. g) The range of elastic moduli of soft human tissues and corresponding PEGgels. Data represent the mean \pm standard deviation ($n = 3$).

human-compatible flexible devices,^[16b] such as wearable sensors, electronic skin, and soft robots.^[34]

2.4. Self-Healing Properties of PEGgels

Physically cross-linked supramolecular networks (based on hydrogen bonding), which usually endow materials fast repair after damage,^[35] have already been used to generate self-healing materials.^[36] Owing to the diffusive nature of multivalent long PEG molecules wrapping around and non-covalently cross-linking the polymer network (Figure 4a), PEGgel dem-

onstrates inherently rapid self-healing properties. To evaluate the self-healing, two PEGgel samples (HAP-5, 3 mm \times 5 mm \times 15 mm) stained with methyl blue and Sudan I were cut into two pieces and re-joined to allow repair (Figure 4b). After 1 min, the repaired gel could support 1 kg without damage (Figure 4c). The mechanical properties of this PEGgel after healing for different time periods are shown in Figure 4d. The tensile stress–strain curves of healed samples overlap almost completely with that of the original samples. After healing for 1 min without any external stimulus, the fracture strain of the sample reached 3600%, demonstrating a self-healing efficiency of $49.1 \pm 8.7\%$ ($n = 3$) measured by dividing the

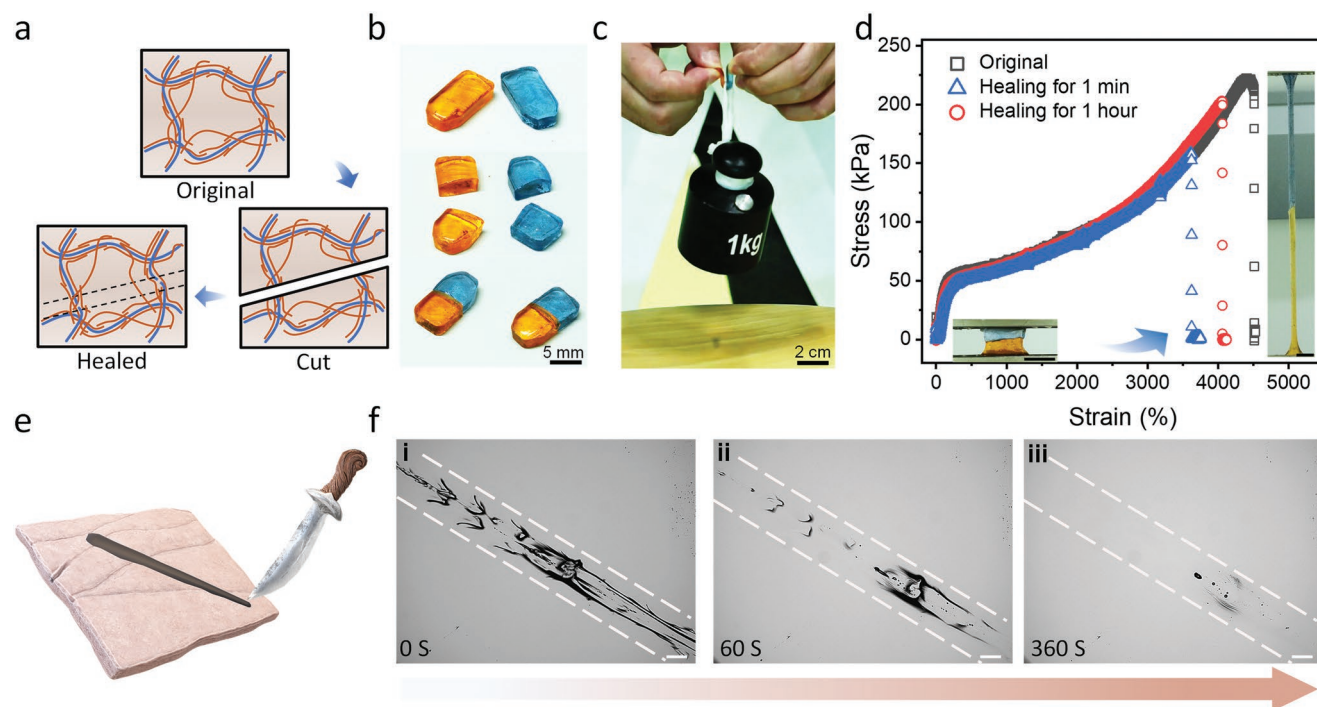


Figure 4. Self-healing properties of PEGgel. a) Self-healing mechanism of the PEGgel is based on the PEG functioning as a diffusive H-bonding molecular glue capable of cross-linking damaged polymer chains. b) The PEGgel (HAP-5) samples (3 mm × 5 mm × 15 mm) stained with methyl blue and Sudan I cut into two pieces show complete healing within 1 min. c) Healed PEGgel sample supports 1 kg weight. d) Tensile stress–strain curves of PEGgel samples after different healing times. Inset photo shows gel stretched over 4000% after 1 h of healing (scale bar: 5 mm). e) Schematic illustration of the scratch-healing test, simulating a skin tissue wound. f) The scratch wound on a PEGgel film (HAP-5, 1000 μm thick) is completely healed after 360 s (scale bar: 500 μm).

toughness of healed samples by the toughness of the original samples. After 1 h of healing, the PEGgel was stretched to 4000% (Figure 4d), representing a self-healing efficiency of $70.2 \pm 3.0\%$ ($n = 3$). After 1 h of healing, the hydrogels and EG gels showed significantly lower self-healing ratios (Figure S15, Supporting Information). For hydrogels (50 vol% water), the self-healing efficiency based on toughness was only 2.7% after 1 min, rising to only 18.5% after 1 h. For EG gels, the self-healing ratio was only 1.3% and 12.2% after 1 min and 1 h of healing time, respectively. The self-healing efficiencies of PEGgels with different PEG ratios were also measured (Table S9, Supporting Information). With a volume fraction of PEG is higher than 35 vol%, the self-healing efficiency of these PEGgels exceeded 50% after healing for 1 h (Figure S16, Supporting Information). After longer time periods, HAP-4.5, HAP-4, HAP-3.5 achieved self-healing efficiencies of $60.9 \pm 0.8\%$ (1 h), $54.9 \pm 6.7\%$ (3 h), and $63.8 \pm 5.0\%$ (6 h), respectively.

We then performed surface scratch recovery tests to simulate skin wound healing (Figure 4e). A razor blade was used to make deep scratches (150–500 μm wide and 1000 μm deep) on a PEGgel film (HAP-5). Optical microscopy images showed noticeable recovery after only 1 min and complete self-healing and disappearance of the wound within 6 min without any external stimulus (Figure 4f and Movie S3: Supporting Information). The same scratch recovery tests were applied to the hydrogels and EG gels with same polymer network and solvent ratio (Figure S17: Supporting Information). After healing for

30 min, only the EG gel showed partial healing, with only the narrow parts of the scratch showing complete recovery. In contrast, only minimal healing of the hydrogel wound occurred. With the same polymer network and solvent ratio, the self-healing speed of PEGgel was significantly higher than that of the EG gel and hydrogel.

Rheology analyses were further used to demonstrate the self-healing process. Strain amplitude sweep was performed to analyze the elastic response of the PEGgel (Figure S18, Supporting Information), and the critical strain regions of storage modulus (G') and loss modulus (G'') were found to be 50% and 100% respectively, which is higher than that of EG gel (30% for G' , 40% for G'') and hydrogel (20% for G' , 30% for G''). The G' value was found to decrease rapidly above the critical strain region, indicating the nonlinear behavior of the gel network involving its damage. Then, the PEGgel was subsequently subjected to a large amplitude oscillatory force (Figure S18d: Supporting Information, 300% strain), and the G' value decreased from ≈ 73.5 to ≈ 45.1 kPa, indicating an impaired network. After decreasing the amplitude (back to 1% strain), the G' recovered (≈ 80 s) to the initial value, and the PEGgel returned to the original state, indicating the quick recovery of the PEGgel inner network, confirming the fast self-recovery capability. For EG gel, the recovery speed was faster than PEGgel (≈ 40 s), resulting from the higher mobility of the polymer chains in EG. But after the amplitude cycling, the EG gel was not able to recover back completely as PEGgel, which may be explained by the weaker long-range interactions. Due to the more fixed

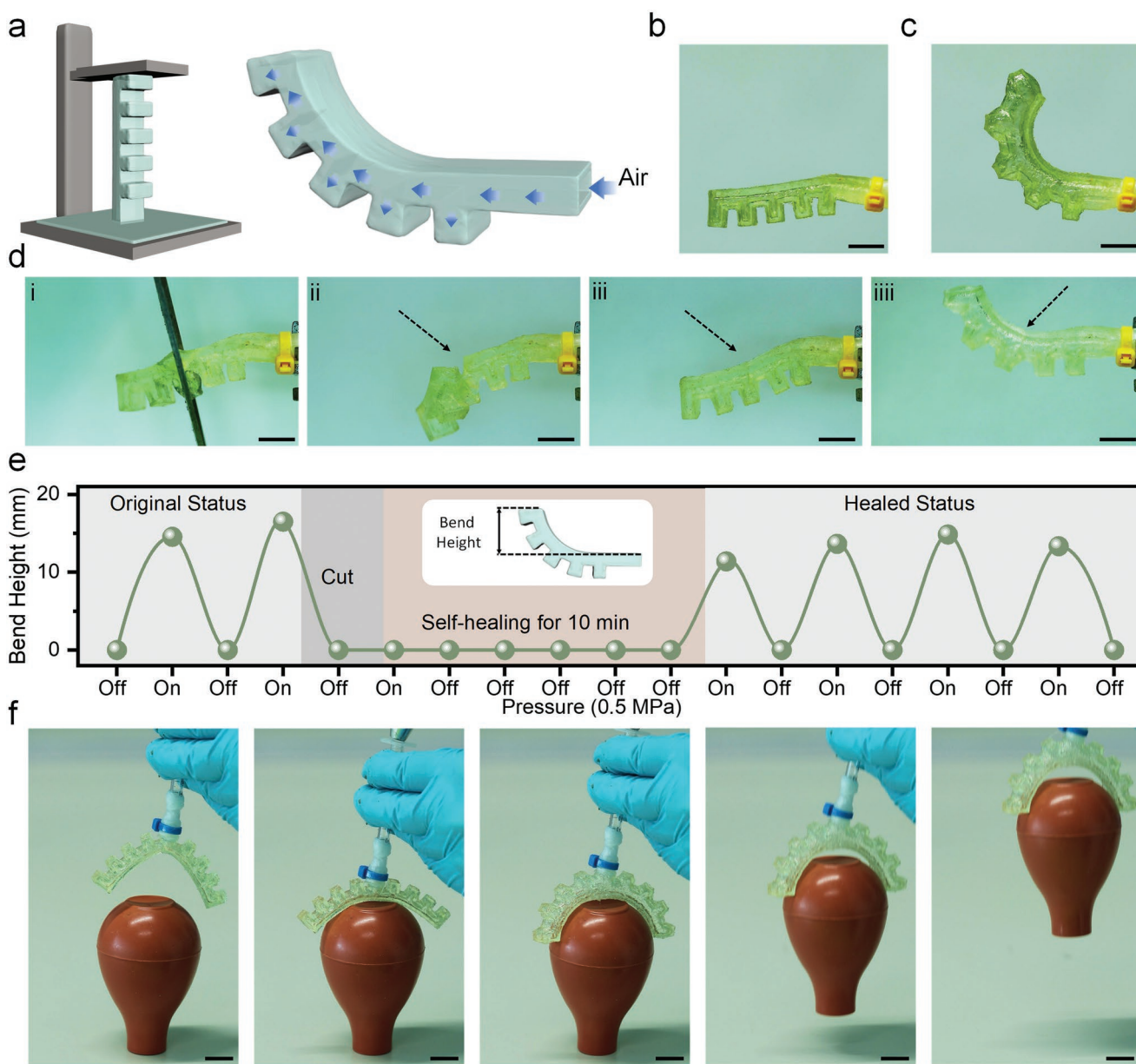


Figure 5. Use of 3D-printable self-healing PEGgel based soft actuators. a,b) Schematic diagram and photographs of a soft pneumatic actuator prepared from HAP-4 via Digital Light Processing (DLP) 3D-printing technology. c) Bending of the 3D-printed actuator under 0.5 MPa air pressure. d) Healing of the actuator after total separation, and bending under 0.5 MPa air pressure after 10 min of healing. e) Quantification of the bend height of the soft actuator before cutting and after healing shows no distinguishable difference. The bend height is the vertical gap between the head and tail. The dotted line connects the data points. f) Design and fabrication of the actuator with two fingers to capture a soft rubber pipette bulb. Scale bars: 5 mm.

polymer network compared with PEGgel and EG gel, hydrogel showed poor self-recovery property under such continuous small–large strain oscillation switch (Figure S18f, Supporting Information).

In summary, the self-healing property of PEGgel is mainly based on: i) mobility of small-molecular weight PEG molecules and the mobility of the polymer network; ii) multivalence of the PEG molecules functioning as dynamic “crosslinkers” utilizing weak multiple H-bonding between main polymer chains.

2.5. Soft Actuators Based on PEGgels

Self-healing soft materials are indispensable for use as soft actuators and robots required to survive in dynamic and complex stress/strain environments in which they are vulnerable to mechanical damage that impairs their performance. To further explore the feasibility of using PEGgels in soft actuators and robots, we fabricated a pneumatic soft actuator through digital light processing (DLP) 3D-printing technology based on HAP-4 gel (Figure 5a). A hollow structure with asymmetry above and

below can be fabricated directly by 3D printing without the need to employ complex and multistep molding or casting manufacturing processes. Thus, this approach enables the geometric complexity and functionality of the soft robots.^[37] When the actuator is pressurized, the sawtooth part expands and deforms toward the non-sawtooth side, which causes a directed force that serves as an actuator. The 3D-printed actuator with a hollow core generated is shown in Figure 5b. When pressure (0.5 MPa) was applied, the actuator bent, and then recovered after the pressure was released (Figure 5c and Movie S4: Supporting Information). Due to the toughness and softness of the PEGgel, the soft actuator obtained was capable of repeatedly supporting a pair of steel scissors weighing 20 g (Figure S19 and Movie S5: Supporting Information), representing 5.4 times its own weight (3.7 g). Since the pneumatic actuators are especially vulnerable to puncture damage, we investigated the self-healing properties of the 3D-printed actuator after it was cut into two pieces (Figure 5d). The ability of the actuator to bend in response to the applied pressure was restored after 10 min of healing (Movie S6, Supporting Information).

In detail, we analyzed the performance of the actuator before cutting and after healing (Figure 5e). The actuator lost deformation ability after complete separation, because of the major leakage of the gas pressure applied. After healing for 10 min, the ability of actuator to bend with applied pressure was restored. Thus, the healing capacity of PEGgels allows the effective repair of damage, and therefore extends the operating lifetime of the actuators. Benefiting from the 3D printability of PEGgels, we further prepared a soft actuator with two fingers (Figure S20, Supporting Information) with the ability to bend into any direction under pressure to capture an object. In a proof-of-concept demonstration, we used the actuator with two fingers to capture a soft rubber pipette bulb. When the pres-

sure was applied, the two fingers of the actuator deformed and held the bulb tightly. Due to the softness of the gel, the bulb was not deformed and was lifted safely (Figure 5f and Movie S7: Supporting Information). In summary, these soft materials based on PEG as a solvent can be easily shaped to form complex structures by 3D printing and heal after severe mechanical damage (scratches and even total separation), thus offering potential for application in the development of soft robots.

2.6. Generality and Customizability

The PEGgel system can be extended to other polymer networks to form gels with better mechanical properties compared with the same network fabricated using hydrogels or EG gels. We used HEMA to prepare hydrogel, EG gel and PEGgel by chemical cross-linking using poly(ethylene glycol) diacrylate (PEGDA, 250 g mol⁻¹, 1 vol% of monomer) (Figure 6a). The obtained PEGgel based on chemically cross-linked PHEMA exhibited a greater fracture strain (400%) compared with the hydrogel with the same polymer network (250%). Importantly, this enhanced performance in stretchability did not sacrifice tensile strength, with the fracture strength of PEGgel (375 kPa) being even slightly higher than that of the hydrogel (350 kPa). However, the EG gel with the same chemical composition as the PEGgel exhibited much weaker mechanical properties, with a fracture strain and tensile strength of 280% and 90 kPa, respectively. As shown in Figure 6b, the chemically cross-linked poly acrylic acid with PEGDA exhibited enhanced strength (from 440 kPa for the hydrogel and 186 kPa for the EG gel to 466 for the PEGgel), fracture strain (535% and 685%, to 1650%), and toughness (1.41 MJ m⁻³ and 0.72 MJ m⁻³, to 3.15 MJ m⁻³). The same phenomenon observed with anionic monomers

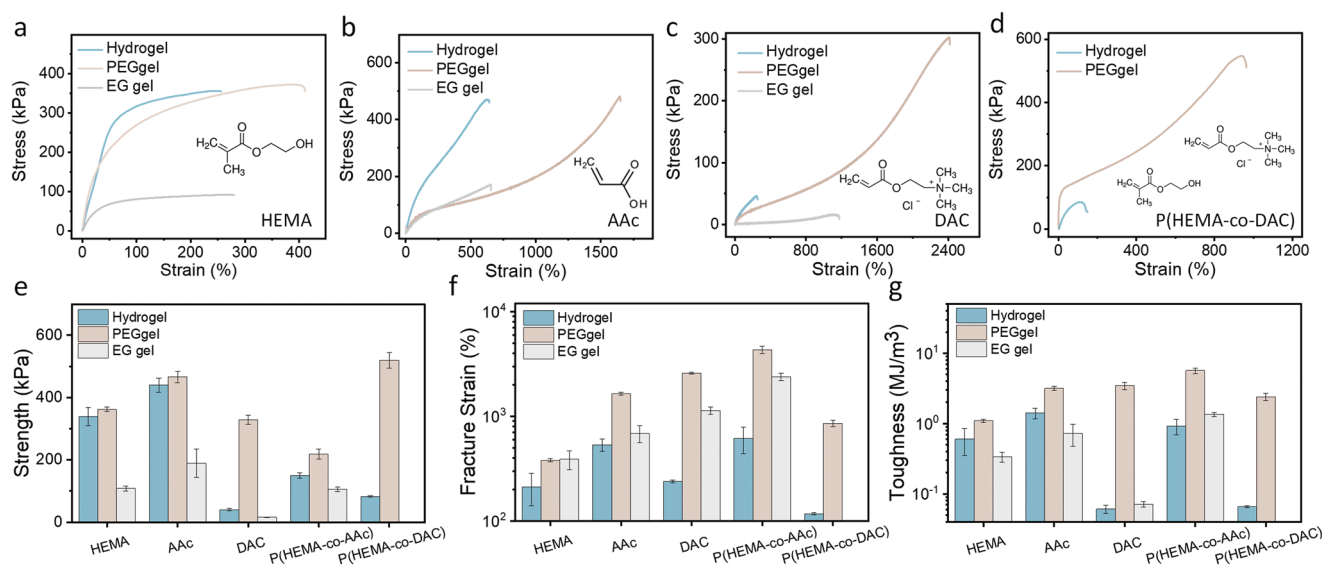


Figure 6. Generality of PEGgel systems in different polymer networks. a–d) Representative stress–strain curves of hydrogel (blue), PEGgel (orange) and EG gel (gray) composed of chemically cross-linked poly(2-hydroxyethyl methacrylate) (a), chemically cross-linked poly(acrylic acid) (b), chemically cross-linked poly([2-(acryloyloxy)-ethyl]-trimethyl ammonium chloride) (c), and a physically cross-linked copolymer of 2-hydroxyethyl methacrylate and [2-(acryloyloxy)-ethyl]-trimethyl ammonium chloride (d). e–g) Strength (e), fracture strain (f), and toughness (g) of three types of gels with various polymer networks. All chemically cross-linked gel is achieving by adding PEGDA (1 vol% of corresponding monomer). Data represent the mean \pm standard deviation ($n = 3$).

occurred, when cationic monomers ([2-(acryloyloxy)-ethyl]-trimethyl ammonium chloride, DAC) were introduced into the PEGgel (Figure 6c). The chemically cross-linked DAC PEGgel showed tensile strength of 329 kPa, which is much higher than the strength of corresponding hydrogel (41 kPa) and EG gel (16 kPa). The toughness also increased from 0.06 MJ m^{-3} (hydrogel) and 0.07 MJ m^{-3} (EG gel) to 3.45 MJ m^{-3} (PEGgel). As shown in Figure 6d, the PEGgel fabricated based on physically cross-linked copolymer of HEMA and DAC exhibited a 5.4-fold increase in tensile strength (from 85 to 547 kPa), a 7-fold increase on fracture strain (from 117% to 938%), and a massive 31-fold increase in toughness (from 0.03 to 1.07 MJ m^{-3}), compared with the corresponding hydrogel. All of the PEGgels with different polymer network demonstrated enhancement on mechanical properties compared with corresponding hydrogels and EG gels. This effect may result from the abundant but relatively weak C–H...O hydrogen bonds between PEG and polymer network. Also, the increased long-range interactions and polymer entanglement facilitated the enhanced durability against fracture. Thus, these findings confirm that the improvement of mechanical property caused by the PEG used as a solvent can be extended to different polymer networks, showing universality and potential in functional soft matter preparation. Since the compatibility between PEG and various polymers has been widely confirmed,^[38] our strategy is not restricted to the systems presented here. We foresee that this approach can be applied to design other tough and functional polymer gels for numerous practical applications.

3. Conclusion

We have developed a universal method for fabrication of tough gels using PEG as a solvent. PEGgels based on P(HEMA-co-AAc) presented superior and versatile properties, in terms of long-lasting performance (>1 month), high stretchability (6000% at 50 mm min^{-1}), transparency (95% for visible light), rapid self-healing (1 min) and 3D printability. A CGMD model revealed that the abundant but relatively weak C–H...O hydrogen bonding added considerably to the overall stiffness of the PEGgel, with the increased long-range correlations and polymer entanglement facilitating the enhanced durability against fracture. Importantly, by changing the volume fraction or molecular weight of PEG, the PEGgel exhibited tunable mechanical properties across a large window of properties with tensile strength increased from 0.22 to 41.3 MPa, fracture strain from 12% to 4336%, elastic modulus from 0.08 to 352 MPa, and toughness from 2.89 to 56.23 MJ m^{-3} . Based on this simple but multi-functional gel, we fabricated self-healing pneumatic actuators, showing potential of PEGgel in broad applications in soft actuators and robots. With the 3D printability, we believe that PEGgels can be integrated easily in other actuator designs and potentially, in other soft systems and machines with different actuation, to generate advanced soft machines. Last but not least, the PEGgel system was successfully applied to other polymer networks, showing generality and customizability. Since the compatibility between PEG and various polymers has been widely confirmed, PEGgels offer great promise for application in various serviceable functions that can be extended

to various platforms to meet the needs of a variety of areas ranging from biomedical applications to flexible electronics and soft robots.

4. Experimental Section

Materials: Acrylic acid, hydroxyethyl methacrylate, [2-(acryloyloxy)-ethyl]-trimethyl ammonium chloride, poly(ethylene glycol) diacrylate, I1173, and I819 were purchased from Sigma–Aldrich (Darmstadt, Germany). All forms of poly(ethylene glycol) were purchased from Thermo Fisher (Schwerte, Germany). Ethanol and acetone were purchased from Merck (Darmstadt, Germany). All chemicals were used as received. All aqueous solutions were prepared with deionized water.

Preparation of Gels: All samples, including hydrogels, EG gels and PEGgels, were prepared by UV-induced one-pot sequential polymerization. Monomers, a photoinitiator, and solvents were mixed in amber bottles. After vortexing for 3 min, a clear solution was obtained. All samples were initiated under 366 nm UV light (6 mW cm^{-2}) for 30 min. The specific prepolymer compositions are shown in Tables S1–S7 (Supporting Information). For PEG1000, the solution mixing was finished at $60 \text{ }^\circ\text{C}$.

3D Printing of PEGgel: The PEGgel containing 40 vol% of PEG 400 and 60 vol% of P(HEMA-co-AAc) was used as the ink for 3D printing with a Digital Light Processing printer (MiiCraft prime 110). I819 was selected for use as the photo initiator at 10 mg mL^{-1} . The curing time for every layer (thickness: $100 \text{ }\mu\text{m}$) was 30 s.

Characterization: The tensile performance of samples was tested using the AGS-X Series Universal Electromechanical Test Frame (Shimadzu Inc., Japan). For tensile tests, samples were molded into a dumbbell shape (thickness, 1–2 mm thick; 2 mm width, 2 mm; length, 8 mm); three samples were prepared for each tensile experiment. The tensile speed was set at 100 mm min^{-1} . The elastic modulus was calculated from the slope of tensile stress–strain curves at 5–10% strain area. The self-healing efficiency was calculated by dividing the toughness of healed samples by the toughness of the original samples. The molecular weight of samples was determined by gel permeation chromatography (GPC) in dimethylacetamide phase (data shown in Table S8, Supporting Information). The differential scanning calorimetry (DSC) measurements were performed on a TA DSC 2500 instrument, in a sealed 40 μL aluminum crucibles under nitrogen atmosphere. Samples with 3–5 mg were analyzed by using a heat/cool/heat cycle with a heating or cooling rate of $20 \text{ }^\circ\text{C min}^{-1}$. In this cyclic thermal measurement, the sample materials were heated from -90 to $150 \text{ }^\circ\text{C}$, then cooled to $-90 \text{ }^\circ\text{C}$ and reheated to $120 \text{ }^\circ\text{C}$. The glass transition temperature (T_g) was determined in the second heat run to eliminate possible interference from the polymer's thermal history. The dynamic viscoelasticity of the samples was measured by ARES G2 (TA Instruments) rheometer via small amplitude oscillatory shear experiments. The samples were placed under a 13 mm-diameter parallel plate. In the strain sweep tests, the shear strain (γ) was from 0.01% to 800% at the frequency of 10 rad s^{-1} and temperature of $25 \text{ }^\circ\text{C}$. In the frequency-sweep tests, the angular frequency (ω) was from 1 to 100 rad s^{-1} at specified temperatures with the shear strain (γ) of 0.5%. The master curves at a reference temperature of $25 \text{ }^\circ\text{C}$ were scaled by time–temperature superposition. The critical strain was defined by the strain point that the modulus starts to decrease on the logarithmic axis.

Coarse-Grain Molecular Dynamic Simulation: CGMD simulations were performed to reproduce initial configurations of the polymer network and investigate the mechanical properties during stretching. A schematic diagram of the CGMD simulations is shown in Figure S10 (Supporting Information). The force-field parameters for the CGMD were fitted to reproduce the tensile stress–strain curves of hydrogel, PEGgel and EG gel based on the same P(HEMA-co-AAc) polymer matrix and 50% solvent fraction (representative curves shown in Figure 1c).

The corresponding CG length λ_{CG} was set at 1 nm and the characteristic molecular mass m_{CG} was set at 100Da. The covalent bonds

in the backbone of P(HEMA-co-AAc) and between the backbone and the side group in HEMA was considered with a bonding strength of 40.0 ϵ_{CG} . Similar to the Kremer-Grest polymer model, the steric repulsion was modeled as a truncated and shifted Lennard-Jones potential. Hydrogen bonding was characterized by the Morse potential. The non-bonded interactions among the different CG beads are listed in Table S10 (Supporting Information).

The polymer chains of P(HEMA-co-AAc) were assigned a fixed length of 600 monomer units, in a random mixture of HEMA:AAc = 36:64. The polymer chains were packed in a $30 \lambda_{CG} \times 30 \lambda_{CG} \times 20 \lambda_{CG}$ simulation box by PACKmol. The corresponding CG bead solvent (water, EG, and PEG) were added to fill the simulation box and went through a simulated annealing process to reach a relaxed state at ambient temperature and pressure.

Upon stretching, the simulation box is elongated in the z-direction whereas in the x-y plane the cross-sectional area shrinks to preserve the overall volume. The stretching is applied every 2000 τ_{CG} with an engineering rate of 0.01 to slowly deform the box dimensions until a 50-times elongation is reached in the z-direction. Average values for the component contributions to the interaction potential of the steric effect, the hydrogen bonds, and the covalent bonds recorded over the last 1000 τ_{CG} during each deformation are shown in Table S10 (Supporting Information). As a limitation of this model, the time series of the energetics showed only minor fluctuations across the whole stretching time span, where critical events, such as the rupture during stretching, can be implied in transitional behaviors for some observables however the definitive critical behaviors cannot be covered. In the post-processing of the MD data, the number of O-H...O and C-H...O hydrogen bonds were calculated based on the Morse potential. The tensile stress σ with respect to the stress tensor in the z-direction was calculated by:

$$\sigma = (1 + \mu)(P - P_{zz}) \quad (1)$$

where μ is the Poisson's ratio, which is estimated to decrease from 0.7 to 0.5 during the elongation in the z-direction.^[39]

NMR Measurement: 2D exchange ^1H -NMR spectra were measured under MAS of 20 kHz for different mixing times in the range from 0–300 ms (Figure 2d–g). The pulse sequence of this experiment is identical to that used in NOESY spectroscopy in solution NMR,^[40] however, the physical mechanisms leading to cross peaks are different in solids or large molecules such as polymers. While in solution NMR of small molecules, cross peaks are caused by cross relaxation, spin diffusion is the dominating mechanism in solids. Cross peaks in solution indicate a proximity (within a distance of ≈ 5 Å) of the spins corresponding to the signals linked by the cross peak. Spin diffusion, however, has a larger distance range as magnetization is exchanging within a larger ^1H -spin network. Cross peaks caused by this effect depend on the ^1H - ^1H dipolar couplings within the spin network, and are influenced by molecular mobility and proximity of the ^1H spins. 2D exchange NMR hence allows to distinguish a compact polymer with reduced local mobility and loose polymer chains, where strong or weak spin diffusion is anticipated, respectively.

Solid-state ^1H NMR measurements were performed using a 500 MHz widebore Bruker Avance III spectrometer. The PEGel, hydrogel and EG gel of copolymer of hydroxyethyl methacrylate and acrylic acid were filled into 3.2 mm rotors and measured within ≈ 1 day after production of the gels. The ^1H -NMR spectra were acquired under magic angle spinning (MAS) with a spinning speed of 20 kHz using a triple-resonant (HCN) MAS probe (Bruker) equipped with a low resonator. A 90°-pulse of 3.2 μs was used. The acquisition time was 20 ms, and 32 scans with a recycle delay of 3 s were averaged in case of the 1D ^1H -NMR spectra. To get insight into the proximities and molecular mobility, 2D exchange experiments were conducted using a NOESY pulse sequence and mixing times of 0, 10, 30, 100, and 300 ms. 400 increments covering 13.33 ppm were used in the indirect dimension, and 8 scans were averaged with a recycle delay of 3 s.

Supporting Information

Supporting Information is available from the Wiley Online Library or from the author.

Acknowledgements

Z.W. is grateful to the China Scholarship Council (CSC) for the Ph.D. scholarship. This project was partly supported by DFG (Heisenbergprofessur Projektnummer: 406232485, LE 2936/9-1). Furthermore, the authors thank the Helmholtz Program “Materials Systems Engineering”, “NACIP (Natural, Artificial and Cognitive Information Processing)” and KIT-Center-Projekt softNeuro 2020 FE.5450.0014.5096 for the support. M.L. and W.W. gratefully acknowledge funding via the Helmholtz Joint Lab of “Virtual Materials Design” (VirtMat). P.A.L., E.S., and W.W. acknowledge the financial support by the DFG under Germany Excellence Strategy via the Excellence Cluster 3D Matter Made to Order (Grant No. EXC-2082/1–390761711) and by the Carl Zeiss Foundation through the “Carl-Zeiss-Focus@HEiKA”. S.G. acknowledges financial support by the DFG instrument grant 121384/58-1. M.H. gratefully acknowledges the support from the “Stiftung der Deutschen Wirtschaft (sdw)” within the Klaus Murmann fellowship.

Open access funding enabled and organized by Projekt DEAL.

Conflict of Interest

The authors declare no conflict of interest.

Data Availability Statement

The data that support the findings of this study are available from the corresponding author upon reasonable request.

Keywords

flexible devices, polymer gels, self-healing materials, soft matter

Received: September 29, 2021

Revised: November 12, 2021

Published online: February 3, 2022

- [1] E. Caló, V. V. Khutoryanskiy, *Eur. Polym. J.* **2015**, *65*, 252.
- [2] a) Y. Liu, J. Liu, S. Chen, T. Lei, Y. Kim, S. Niu, H. Wang, X. Wang, A. M. Foudeh, J. B. H. Tok, Z. Bao, *Nat. Biomed. Eng.* **2019**, *3*, 58; b) Z. Wang, Y. Cong, J. Fu, *J. Mater. Chem. B* **2020**, *8*, 3437.
- [3] T. Li, G. Li, Y. Liang, T. Cheng, J. Dai, X. Yang, B. Liu, Z. Zeng, Z. Huang, Y. Luo, T. Xie, W. Yang, *Sci. Adv.* **2017**, *3*, 1602045.
- [4] a) Y. S. Zhang, A. Khademhosseini, *Science* **2017**, *356*, eaaf3627; b) S. Correa, A. K. Grosskopf, H. L. Hernandez, D. Chan, A. C. Yu, L. M. Stapleton, E. A. Appel, *Chem. Rev.* **2021**, *18*, 11385; c) H. Yuk, S. Lin, C. Ma, M. Takaffoli, N. X. Fang, X. Zhao, *Nat. Commun.* **2017**, *8*, 14230.
- [5] O. Wichterle, D. Lim, *Nature* **1960**, *185*, 117.
- [6] X. Liu, J. Liu, S. Lin, X. Zhao, *Mater. Today* **2020**, *36*, 102.
- [7] H. Yang, M. Ji, M. Yang, M. Shi, Y. Pan, Y. Zhou, H. J. Qi, Z. Suo, J. Tang, *Matter* **2021**, *4*, 1935.
- [8] a) K. Y. Lee, D. J. Mooney, *Chem. Rev.* **2001**, *101*, 1869; b) K. T. Nguyen, J. L. West, *Biomaterials* **2002**, *23*, 4307.

- [9] J. Guo, X. Liu, N. Jiang, A. K. Yetisen, H. Yuk, C. Yang, A. Khademhosseini, X. Zhao, S.-H. Yun, *Adv. Mater.* **2016**, *28*, 10244.
- [10] C. Yan, D. J. Pochan, *Chem. Soc. Rev.* **2010**, *39*, 3528.
- [11] Y. Kim, H. Yuk, R. Zhao, S. A. Chester, X. Zhao, *Nature* **2018**, *558*, 274.
- [12] X. Zhao, X. Chen, H. Yuk, S. Lin, X. Liu, G. Parada, *Chem. Rev.* **2021**, *121*, 4309.
- [13] a) H. Kamata, Y. Akagi, Y. Kayasuga-Kariya, U.-i. Chung, T. Sakai, *Science* **2014**, *343*, 873; b) T. Sakai, T. Matsunaga, Y. Yamamoto, C. Ito, R. Yoshida, S. Suzuki, N. Sasaki, M. Shibayama, U.-i. Chung, *Macromolecules* **2008**, *41*, 5379; c) X. Huang, S. Nakagawa, X. Li, M. Shibayama, N. Yoshie, *Angew. Chem., Int. Ed.* **2020**, *59*, 9646.
- [14] a) J. P. Gong, Y. Katsuyama, T. Kurokawa, Y. Osada, *Adv. Mater.* **2003**, *15*, 1155; b) X. Zhao, *Soft Matter* **2014**, *10*, 672; c) J.-Y. Sun, X. Zhao, W. R. K. Illeperuma, O. Chaudhuri, K. H. Oh, D. J. Mooney, J. J. Vlassak, Z. Suo, *Nature* **2012**, *489*, 133.
- [15] E. Prince, E. Kumacheva, *Nat. Rev. Mater.* **2019**, *4*, 99.
- [16] a) M. Hua, S. Wu, Y. Ma, Y. Zhao, Z. Chen, I. Frenkel, J. Strzalka, H. Zhou, X. Zhu, X. He, *Nature* **2021**, *590*, 594; b) S. Wu, M. Hua, Y. Alsaïd, Y. Du, Y. Ma, Y. Zhao, C.-Y. Lo, C. Wang, D. Wu, B. Yao, J. Strzalka, H. Zhou, X. Zhu, X. He, *Adv. Mater.* **2021**, *33*, 2007829.
- [17] N. Gao, Y. He, X. Tao, X.-Q. Xu, X. Wu, Y. Wang, *Nat. Commun.* **2019**, *10*, 547.
- [18] Z. Cao, H. Liu, L. Jiang, *Mater. Horiz.* **2020**, *7*, 912.
- [19] L. Han, K. Liu, M. Wang, K. Wang, L. Fang, H. Chen, J. Zhou, X. Lu, *Adv. Funct. Mater.* **2018**, *28*, 1704195.
- [20] Q. Rong, W. Lei, L. Chen, Y. Yin, J. Zhou, M. Liu, *Angew. Chem., Int. Ed.* **2017**, *56*, 14159.
- [21] F. Chen, D. Zhou, J. Wang, T. Li, X. Zhou, T. Gan, S. Handschuh-Wang, X. Zhou, *Angew. Chem., Int. Ed.* **2018**, *57*, 6568.
- [22] F. E. Bailey, *Poly(ethylene oxide)*, Academic Press, New York **1976**.
- [23] In *Poly(Ethylene Glycol) Chemistry: Biotechnical and Biomedical Applications*, (Ed: J. M. Harris), Springer, Topics in Applied Chemistry, Boston, MA, USA **1992**.
- [24] J. Chen, S. K. Spear, J. G. Huddleston, R. D. Rogers, *Green Chem.* **2005**, *7*, 64.
- [25] a) J. Mattia, P. Painter, *Macromolecules* **2007**, *40*, 1546; b) M. M. Coleman, D. J. Skrovanek, J. Hu, P. C. Painter, *Macromolecules* **1988**, *21*, 59.
- [26] M. Kozłowska, J. Goclon, P. Rodziewicz, *ChemPhysChem* **2016**, *17*, 1143.
- [27] S. Elaheh, L. Modan, W. Wolfgang, *Res. Square* **2021**, <https://doi.org/10.21203/rs.3.rs-151096/v1>.
- [28] M. Kröger, *Comput. Phys. Commun.* **2005**, *168*, 209.
- [29] In *Biosurfaces: A Materials Science and Engineering Perspective*, (Eds: K. Balani, V. Verma, A. Agarwal, R. Narayan), John Wiley & Sons, Hoboken, NJ, USA **2014**, <https://doi.org/10.1002/9781118950623.app1>; b) H. R. Brown, T. P. Russell, *Macromolecules* **1996**, *29*, 798.
- [30] a) J. Qin, S. T. Milner, *Macromolecules* **2014**, *47*, 6077; b) T. Stauch, A. Dreuw, *Angew. Chem., Int. Ed.* **2016**, *55*, 811.
- [31] E. Zhang, R. Bai, X. P. Morelle, Z. Suo, *Soft Matter* **2018**, *14*, 3563.
- [32] a) T. R. Cox, J. T. Erler, *Dis. Models Mech.* **2011**, *4*, 165; b) D. T. Butcher, T. Alliston, V. M. Weaver, *Nat. Rev. Cancer* **2009**, *9*, 108.
- [33] S. Diridollou, V. Vabre, M. Berson, L. Vaillant, D. Black, J. M. Lagarde, J. M. Grégoire, Y. Gall, F. Patat, *Int. J. Cosmet. Sci.* **2001**, *23*, 353.
- [34] D. Qi, K. Zhang, G. Tian, B. Jiang, Y. Huang, *Adv. Mater.* **2021**, *33*, 2003155.
- [35] A. Pena-Francesch, H. Jung, M. C. Demirel, M. Sitti, *Nat. Mater.* **2020**, *19*, 1230.
- [36] a) P. Cordier, F. Tournilhac, C. Soulié-Ziakovic, L. Leibler, *Nature* **2008**, *451*, 977; b) Y. Chen, A. M. Kushner, G. A. Williams, Z. Guan, *Nat. Chem.* **2012**, *4*, 467.
- [37] D. K. Patel, A. H. Sakhaei, M. Layani, B. Zhang, Q. Ge, S. Magdassi, *Adv. Mater.* **2017**, *29*, 1606000.
- [38] a) M. Zhang, X. H. Li, Y. D. Gong, N. M. Zhao, X. F. Zhang, *Biomaterials* **2002**, *23*, 2641; b) A. K. Mohapatra, S. Mohanty, S. K. Nayak, *Polym. Compos.* **2014**, *35*, 283; c) W. R. Rolim, J. C. Pieretti, D. L. S. Renó, B. A. Lima, M. H. M. Nascimento, F. N. Ambrosio, C. B. Lombello, M. Brocchi, A. C. S. de Souza, A. B. Seabra, *ACS Appl. Mater. Interfaces* **2019**, *11*, 6589.
- [39] a) J. Liu, S. Wu, L. Zhang, W. Wang, D. Cao, *Phys. Chem. Chem. Phys.* **2011**, *13*, 518; b) L. Wang, H. Liu, F. Li, J. Shen, Z. Zheng, Y. Gao, J. Liu, Y. Wu, L. Zhang, *Phys. Chem. Chem. Phys.* **2016**, *18*, 27232.
- [40] J. Jeener, B. H. Meier, P. Bachmann, R. R. Ernst, *J. Chem. Phys.* **1979**, *71*, 4546.